Wirelessly Powered Drug-free and Anti-infective Smart Bandage for Chronic Wound Care

Irfan Ullah, *Member, IEEE*, Mahmoud Wagih, *Member, IEEE*, Yixuan Sun, Yi Li, Kata Hajdu, Rémi Courson, Catherine Dreanno, Enora Prado, Abiodun Komolafe, *Member, IEEE*, Nick R. Harris, *Senior Member, IEEE*, Neil M. White, *Senior Member, IEEE*, and Steve Beeby, *Fellow, IEEE*

***Abstract*— We present a wirelessly powered ultraviolet-C (UVC) radiation-based disinfecting bandage for sterilization and treatment in chronic wound care and management. The bandage contains embedded low-power UV light-emitting diodes (LEDs) in the 265 to 285 nm range with the light emission controlled via a microcontroller. An inductive coil is seamlessly concealed in the fabric bandage and coupled with a rectifier circuit to enable 6.78 MHz wireless power transfer (WPT). The maximum WPT efficiency of the coils is 83% in free space and 75% on the body at a coupling distance of 4.5 cm. Measurements show that the UVC LEDs are emitting radiant power of about 0.6 mW and 6.8 mW with and without fabric bandage, respectively, when wirelessly powered. The ability of the bandage to inactivate microorganisms was examined in a laboratory which shows that the system can effectively eradicate Gram-negative bacteria, *Pseudoalteromonas* sp. D41 strain, on surfaces in six hours. The proposed smart bandage system is low-cost, battery-free, flexible and can be easily mounted on the human body and, therefore, shows great promise for the treatment of persistent infections in chronic wound care.**

***Index Terms*— Smart bandage, UVC LED, e-textiles, wearables, battery-less, wireless power transfer, inductive coil, chronic wound care.**

I. INTRODUCTION

CHRONIC non-healing wounds require continuous monitoring and special care to heal. Chronic wound healing disorders are a common problem in older adults, diabetic and obese patients [1]. With the increase in the ageing population, chronic non-healing wounds present a major economic burden

This work was supported by European Regional Development Fund (ERDF) via its Interreg V France (Channel) England programme: Smart Textile for Regional Industry and Smart Specialization Sectors (SmartT) and EPSRC project "Functional electronic textiles for light emitting and colour changing applications" (EP/S005307/1). M. Wagih was supported by the Royal Academy of Engineering and the Office of the Chief Science Adviser for National Security under the UK Intelligence Community Research Fellowship programme. The work of S. Beeby was supported by the Royal Academy of Engineering under the Chairs in Emerging Technologies Scheme.

I. Ullah, Y. Sun, Y. Li, A. Komolafe, N. R. Harris, N. M. White and S. Beeby are with the School of Electronics and Computer Science, University of Southampton, Southampton, SO17 1BJ, U.K. (email: i.ullah@soton.ac.uk).

M. Wagih is with the James Watt School of Engineering, University of Glasgow, Glasgow, G12 8QQ, U.K. (email: mahmoud.wagih@glasgow.ac.uk).

K. Hajdu, R. Courson, C. Dreanno and E. Prado are with Detection, Sensors and Measurements Laboratory, Ifremer, Brest, France (e-mail: enora.prado@ifremer.fr).

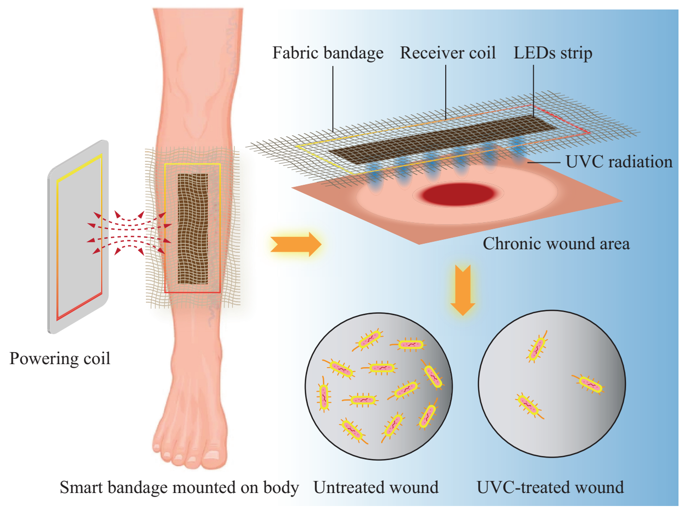

Fig. 1: The proposed battery-free smart bandage can be used for treating wound surfaces.

to healthcare systems and also significantly affect the quality of life of an individual [2], [3]. To date, the treatment of chronic wounds involves frequent cleaning with saline solutions, removal of necrotic tissue and changing of dressings [4]–[6]. These approaches to chronic wound cleaning may not be effective for all types of chronic wounds if they are not complemented with other forms of wound treatment. For example, using normal saline for wound cleansing alone has been found to be ineffective in reducing wound bioburden and may even impede wound healing, especially in wounds with high bacterial load [7].

Wound healing is complicated when a bacterial infection is present either due to highly exudate wounds or the lack of a moist environment that may happen when non-occlusive dressings are used. To address this issue, new bandage systems that include passive and stimulus-activated delivery mechanisms have been developed to localize the supply of antibiotics and antibacterial treatment to the wound within the bandage as discussed in review papers [8]–[11]. The bandage material for passive drug delivery is usually functionalized by coating textile fibers with antibacterial polymers [12], [13] or nanoparticles [14], [15], which limit bacterial growth when in contact with the wound [8], [10]. However, the added functionality can

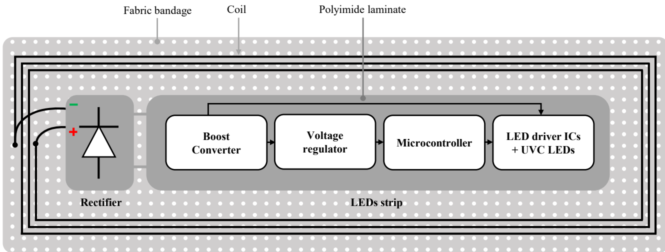

Fig. 2: Block diagram of the wirelessly powered chronic wound disinfection smart bandage.

affect the mechanical properties of such bandages [10], and the main limitation of this delivery method is the lack of control over the delivered drug dosage. Stimulus-activated delivery of antibiotics, on the other hand, helps to control the drug dosage supplied to the wound. Encapsulated antibiotics within the bandages are released into the wound in response to changes in wound biomarkers, such as temperature, oxygen level, pH level, and biofilms, through activation mechanisms like UV radiation [16]and heaters [9]. In some cases, microneedles are used for invasive drug delivery to the dermal layer within the skin [17]. One significant limitation of all such bandages is the limited supply of antibacterial ointment or antibiotics for bacterial treatment throughout the wound healing process. Additionally, the increasing antibiotic resistance associated with non-responsive and drug-resistant bacterial strains that emerge from indiscriminate or excessive use of antibiotics highlights the need for developing new smart bandages that incorporate a non-antibiotic process for inactivating bacteria and preventing bacterial growth at wound sites.

To achieve more effective wound care without over-reliance on antibiotics, there is an urgent need to develop an alternative antimicrobial approach for treating infected wounds. For example, [18] discusses the use of ultraviolet (UV) radiation within the C bandwidth (200 to 280 nm) for treating infections and its effects on wound healing. In this study, we present the first wearable and battery-free smart bandage that utilizes UVC light-emitting diodes (LEDs) [19], enabling an antibiotic-free, low-cost alternative dressing that provides wound disinfection.

UVC radiation is highly antimicrobial and has been widely used for microbial inactivation in water purification, food contact surfaces and medical equipment [20]. In [21], the inactivation of different microorganisms in water was investigated by using various wavelength combinations across UVA (315–400 nm), UVB (280–315 nm) and UVC (200–280 nm). It was observed that the combinations of UVC and UVB LEDs always achieved microbial inactivation, but UVA may improve or reduce *E. coli* inactivation depending on the manner of application such as applying UVA after UVC/UVB, applying UVA before UVC/UVB or applying UVA only. Similarly, the effect of UV light on microbial inactivation in apple juice is described in [22]. This showed that exposing apple juice to UV light for short periods of time achieved a reduction in *E. coli* and *L. innocua* to below detection limits while having marginal effects on physical, chemical, and sensory (taste and odour) properties. Additionally, recent research shows that UVC-based irradiation has the potential to efficiently inactivate diverse forms of coronaviruses such as MERS CoV, SARS CoV-1, and SARS CoV-2 and is therefore an efficient tool for controlling the transmission of coronaviruses [23]. The successful use of UV light in the treatment of wounds has been demonstrated in many cases [24]–[27]. The exposure of skin to UVC has also been shown to inactivate methicillin-resistant Staphylococcus aureus (MRSA) which can cause serious postoperative infections [28]. The radiation doses applied were in the range of 15–40 mJ/cm^2 which were found to have a negligible effect on healthy skin cells. The ability of UV radiation to treat antibiotic-resistant microbial species without inducing further resistance is a highly attractive feature of the approach [29]. Care should be taken to ensure host cells are not affected by the exposure and hence it is important to be able to control dosage in terms of intensity and duration. Short wavelength UVC in the range of 200 to 230 nm can be regarded as safe due to the inability of the radiation at these wavelengths to penetrate host eukaryotic cells [29]. In vivo irradiation with 222 nm UVC was found to reduce MRSA bacteria in infected wounds without damaging either epidermal or dermal cells [30]. The UVC radiation does not need to have pinpoint millimeter accuracy for antibacterial action. Instead, the wavelength, intensity, time and frequency are crucial parameters to ensure treatment efficiency. The position and the design of the UVC LED will need to be optimized within the bandage to control the efficiency and limit illumination on the boundary. This will depend on the size and geometry of the bandage.

Smart bandages can provide important information about the wound healing process by continuous monitoring, in real-time, key parameters in the wound such as temperature, moisture level, pH level and wound oxygenation [31]–[34]. In [35] a battery-powered inkjet printed smart bandage was demonstrated wirelessly monitoring irregular bleeding, variations in pH levels, and external pressure at the wound site. The bandage operated at around 2.4 GHz utilizing the IEEE 802.15.4 standard to transmit data to an external device. Alternatively, a Near-field Communication (NFC)-based smart bandage for wireless strain and temperature sensing was proposed in [36]. The bandage is battery-free and operates from the energy harvested from the NFC reader.

Removing the requirement for a battery is highly desirable since they have a finite lifetime, are rigid, environmentally unfriendly, and require frequent recharging or replacement [37]. NFC was primarily designed to wireless information or data transfer in close proximity. Consequently, the circuitry designed for data transfer is not optimised for efficient power transfer between devices and limits the maximum power level which can be delivered. Therefore, all electronic treatment bandages reported relied on a battery and could not be sustained using wireless power transfer based on NFC. Furthermore, radiative wireless power transfer in the far-field can be used for the transmission of power over long distances, as proposed in [49]. However, all reported wearable far-field WPT systems have an output under 10 mW [50], which would be insufficient to power a therapeutic smart bandage. An alternative to NFC is magnetic resonant (MR) wireless power transfer (WPT), which operates at 6.78 MHz [38]–

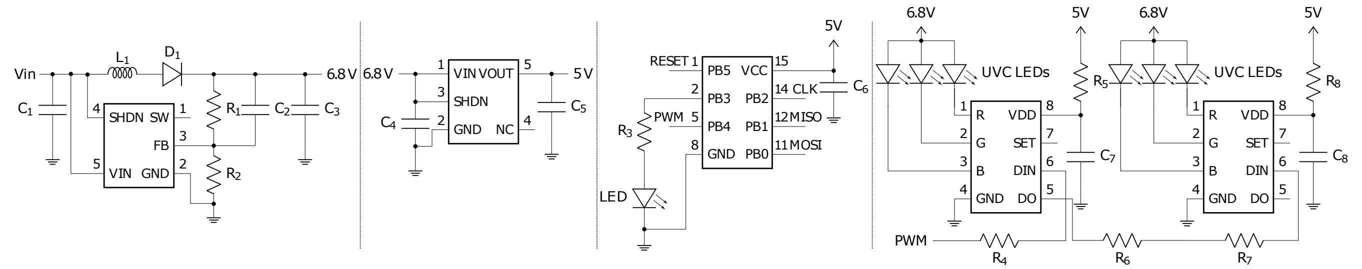

Boost converter | Voltage regulator | Microcontroller | LEDs driver ICs + UVC LEDs

Fig. 3: Schematic representation of the UVC LEDs strip for the chronic wound smart bandage system.

[42]. A magnetic resonant three-coil WPT system operating at 6.78 MHz for wearable devices is proposed in [43], showing that the system has power transfer efficiency of 50% and 60% at Tx and Rx separation distances of 1 cm and 4 cm on the human body and in the air, respectively. Alternatively, a compact flexible, wearable resonant inductive WPT system was proposed in [44] that achieved a power efficiency of 80% over a relatively long range of 60 mm. Recently, an all-textile-based 6.78 MHz WPT receiver was demonstrated with a power output exceeding 3 W [45]. Textile-based, flexible and wearable WPT coils have been realized using inkjet printing [46], embroidery [47], and adhesive-backed copper wires [48].

This paper presents a battery-free wound-treatment anti-infective smart bandage, powered from a 6.78 MHz resonant WPT; the circuit filament and textile coil are concealed within a standard fabric bandage. The low-power UVC LED circuit filament was tested on a *Pseudoalteromonas* sp. D41 bacterial strain, a Gram-negative bacteria, demonstrating a three-fold reduction in the bacterial growth, compared to an untreated strain culture, from light intensities as low as 10 µW. The paper is organized as follows: Section II details the overall system design, Section III presents the simulation and measurement results of the WPT system and Section IV describes the anti-bacterial properties of the bandage. Finally, Section V concludes the paper.

II. System Design

The block diagram of the anti-infective smart bandage is shown in Fig. 2 and comprises of three elements: (i) an inductive coil, (ii) a voltage doubler rectifier, and (iii) a UVC LEDs strip (Fig. 3). The coil is designed and coupled with the rectifier circuit to efficiently capture the wireless power from the resonant electromagnetic field generated by the transmitter coil. The rectifier circuit feeds the dc-dc boost converter on the LED strip which steps up the low voltage into the higher voltage of 6.8 V required to power the UVC light-emitting diodes. The UVC LEDs emit light in the wavelength range of 265 to 285 nm to inactivate the bacteria on the wound surface.

A. Coil Designs

Rectangular transmitter (Tx) and receiver (Rx) coils were fabricated using a 0.36 mm-thick silk-coated copper Litz wire [51]. Both coils are 200 mm long and 65 mm wide, as shown in Fig. 5. The gap between adjacent turns is 2 mm and 4 different coils with 3, 5, 7 and 8 turns were simulated and fabricated. A PFAFF Creative 3.0 sewing machine was used to embroider the Litz wire onto a fabric bandage [52]. The fabric bandage has a relative permittivity (ϵ_r) of 1.2, loss tangent (tan δ) of 0.02 and a thickness of 1.2 mm. The value of the tuning capacitor C is calculated as follows [19]:

$$C = \frac{1}{4\pi^2 f_r^2 L} \quad (1)$$

where L is the inductance of the coil and f_r is the resonance frequency:

$$f_r = \frac{1}{2\pi\sqrt{LC}}. \quad (2)$$

Coil properties are given in Table I where the inductance L of the coils was measured at 6.78 MHz using a Rohde & Schwarz ZVB4 impedance analyser while lumped capacitor value was calculated using (1). The quality factor Q was calculated using the following equation:

$$Q = \frac{2\pi f_r L}{R}. \quad (3)$$

Fig. 4 illustrates the process of fabricating fabric bandage coils using an embroidery technique. First, a CAD file was created using Autodesk Eagle [53] and then transformed into a digitized design using the 6D embroidery system. The fabric bandage was affixed to a firm fusible interlining [54] using an adhesive spray [55] and placed in the embroidery frame, which was then connected to the embroidery machine [56]. The Litz wire was wound onto a bobbin, and the assistant thread was put in a spool holder on the machine. The stitching tension between the coil and the thread onto the bandage is controlled by the embroidery setup parameters, as depicted in Fig. 4.

B. Rectifier Circuit

The rectifier circuit is based on a voltage doubler topology, (shown in Fig. 6) which uses two 1000 pF capacitors and two silicon carbide Schottky diodes from GeneSiC semiconductor [57] with repetitive peak reverse voltage of 1200 V and continuous forward current of 1 A [58]. The input of the circuit is connected to the receiver coil while the outputs are connected to the dc-dc boost converter of the LEDs strip. There is a slot in the rectifier layout for a tuning capacitor for the coil.

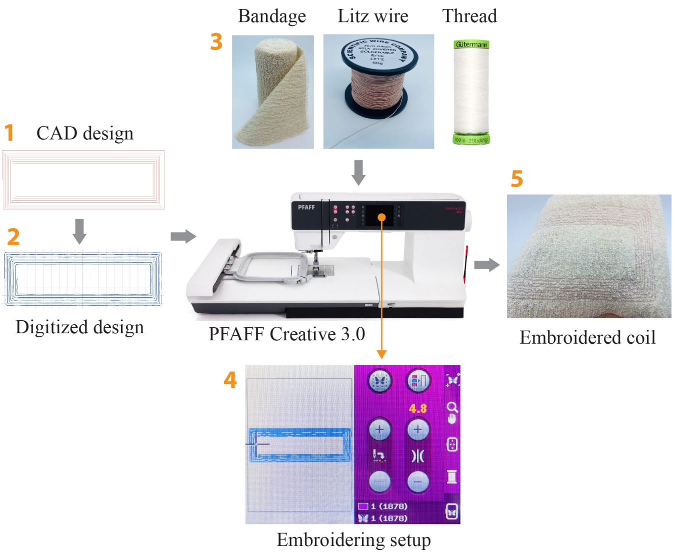

Fig. 4: Embroidering process for fabricating all fabric bandage coils.

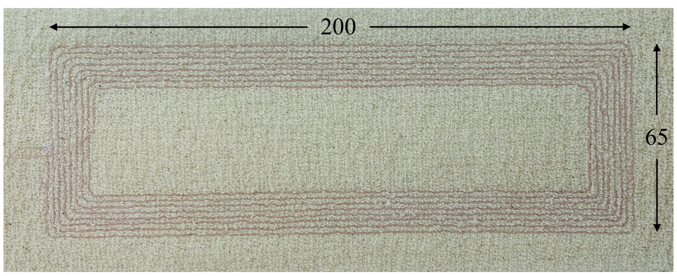

Fig. 5: Prototype of the transmitter coil design of 8 turns manufactured by embroidered silk-coated copper Litz wire into a fabric bandage. (Dimensions are in mm)

C. UVC LEDs Strip

Fig. 3 depicts the schematic diagram of the LEDs strip which consists of a dc-dc boost converter, a voltage regulator, a microcontroller, LED driver ICs and UVC emitting diodes. The assembled circuit is shown in Fig. 7a. The LM2704 [59] step-up dc-dc boost converter with a 550 mA peak current limit is used to adjust the output voltage to 6.8 V. The input range of the converter is 2.2 to 7 V, and the adjustable output voltage is up to 20 V. The output voltage (6.8 V) can be set by selecting values for R_1 and R_2 using the following equation:

TABLE I: Measured inductance and resistance of the coil designs. The capacitance value was calculated using (1).

	$3\ turns$	$5\ turns$	$7\ turns$	$8\ turns$
L (μH)	3.87	8.98	14.02	17.99
R (Ω)	4.41	6.55	7.17	9.10
C (pF)	142.12	61.35	39.46	30.62
Q	37.38	58.40	83.29	84.21

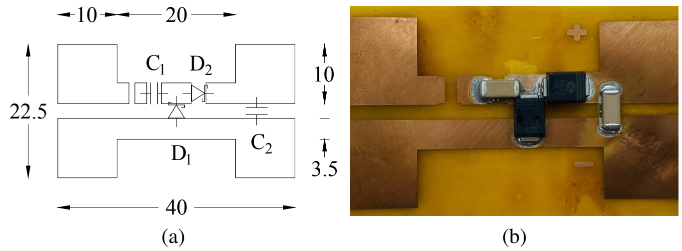

Fig. 6: Voltage doubler rectifier circuit: (a) geometry, and (b) fabricated prototype. (Dimensions are in mm)

$$R_1 = R_2 \left(\frac{v_{out}}{1.237\ V} - 1 \right). \tag{4}$$

A 4.7 pF capacitor is used as to smooth the input signal. Similarly, a low equivalent series resistance (ESR) capacitor of 4.7 pF is used for the output to minimize output voltage ripple.

The ATtiny85 from Microchip [60] is used to control the brightness of the LEDs, operating at a voltage between 1.8 V and 5.5 V. The microcontroller required a lower voltage than the UVC sources and a MCP1801 [61] voltage regulator is used to supply the microcontroller. The regulator converts the input voltage from 6.8 V and to an output voltage of 5 V.

The UVC LED (VLMU35CL2-275-120) [62] is a ceramic packaged low-power LED (see Fig. 7b) with a radiant power of typically 3 mW at 20 mA in a wavelength range of 265 to 285 nm. The brightness of the LEDs is controlled via the microcontroller and the WS2811 NeoPixel LED driver chip [63] using the pulse width modulation (PWM) technique. The forward voltage of the light-emitting diode is between 5 to 8 V. By placing the UVC LEDs on one side of the strip and controlling the distance between them, it is possible to precisely control light emission and achieve optimal UVC irradiance. This can ensure that the wound surface receives an appropriate amount of UV radiation.

D. Fabrication and Encapsulation

In order to achieve the level of flexibility required in the smart bandage application, the circuit was fabricated on a 25 μm-thick polyimide copper-coated film (Fig. 7c). The total size of the strip is 150 mm × 20 mm. The flexible strip was patterned using standard photolithography and etching processes, following the design rules presented in [64].

After soldering the components, a novel vacuum forming method was used to encapsulate the flexible LEDs strip using a Formech 450 DT as described in [65], [66]. A flexible and breathable thermoplastic encapsulant, Platilon®U [67], was used to seal the circuit. Whilst this protects the circuit mechanically and from moisture such as wound exudate but was also found to be opaque to UV wavelengths and therefore windows were cut out over the LEDs. A cross-section of the encapsulated circuit is shown in Fig. 7d.

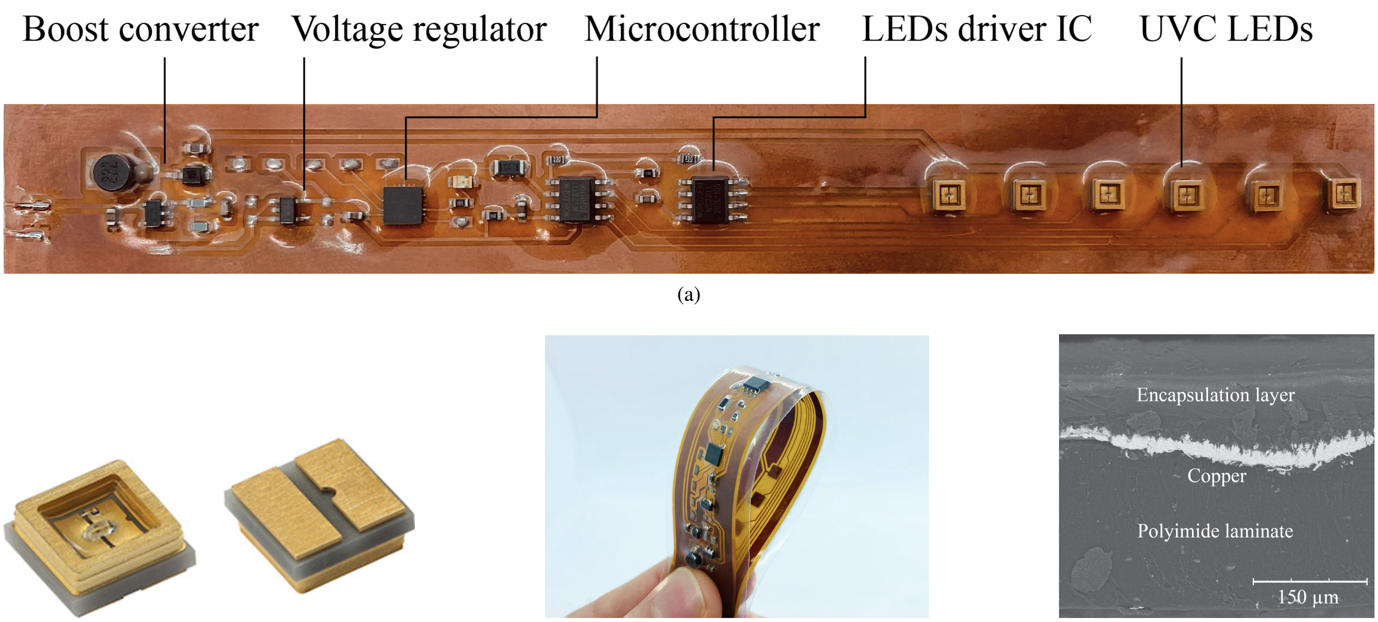

Fig. 7: (a) Fabricated prototype of the UVC LEDs strip for smart bandage; (b) Photograph of a 265 to 285 nm ceramic packaged low power LED with silicone lens device (footprint = 3.45 mm ×3.45 mm × 1.38 mm, top isometric view (left) and bottom isometric view (right); (c) Fully flexible circuit; (d) Scanning electron microscope photo of the cross-section of the encapsulated circuit

III. Simulation and Measurement Results

A. Rectifier Characterization

To evaluate the performance of the rectifier, the rectifier was connected to the power amplifier and a 250 Ω power resistor was attached to the output terminal of the rectifier. Additionally, a 4.7 µF smoothing capacitor was deployed at the rectifier output terminal. The power amplifier received input power ranging from 10 to 40 dBm, and the DC voltage across the resistive load was measured with an oscilloscope. Fig. 8 illustrates the RF-to-DC efficiency and output DC voltage against RF input power from 10 to 40 dBm. The results indicate that the maximum rectifier efficiency of 91% was achieved at an input power of 40 dBm. Additionally, we measured the efficiency after encapsulating the rectifier in a polyimide coating. As shown in Fig. 8, the encapsulation did not significantly impact the RF-to-DC power efficiency of the system.

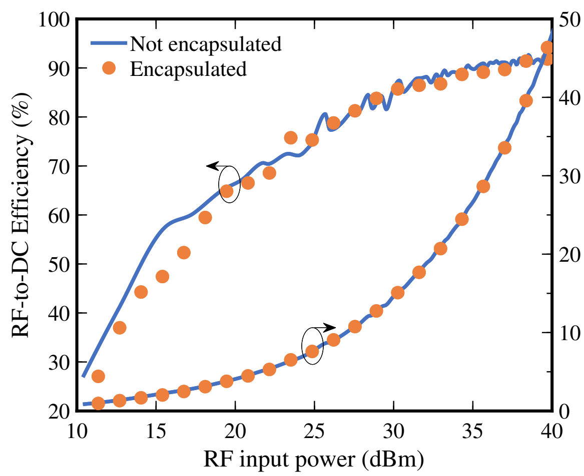

Fig. 8: Measured RF-to-DC efficiency and output voltage against RF input power from 10 to 40 dBm for load impedance of 250 Ω.

B. WPT Efficiency

Four coils of 3 to 8 turns were tested to study the optimal coil turns ratio for efficient power transfer. The following experimental conditions were also investigated with Comsol Multiphysics (Fig. 9) providing simulated WPT efficiency for the following arrangements. The capacitor value given in Table I was connected in series with the coil to tune the resonance frequency to 6.78 MHz. The WPT efficiency of the coils was investigated with a two ports vector network analyzer (VNA), Rhode & Schwarz ZVB4, as shown in Fig. 9a. The separation distance between the transmitter and receiver coil is denoted by *d*. Both coils were aligned in the coaxial direction and the distance d was varied from 1 to 10 cm, in 0.5 cm steps. The S_{21} of the coils in free space and on the body was measured for varying *d*, with the efficiency given by $\eta_{WPT} = |S_{21}|^2$.

In the first experiment, the WPT efficiency between the Tx coil of 8 turns and the Rx coils of 3 to 8 turns was investigated, as shown in Fig. 9b. It can be observed that at an operating distance of 4.5 cm, the wireless power transfer efficiency of the Rx coil of 3 turns is about 83.3% in free space. As the separation distance between coils increases, the efficiency gradually decreases. The Rx coils with 5, 7 and 8 turns have higher efficiency than the 3 turns coil at separation distances

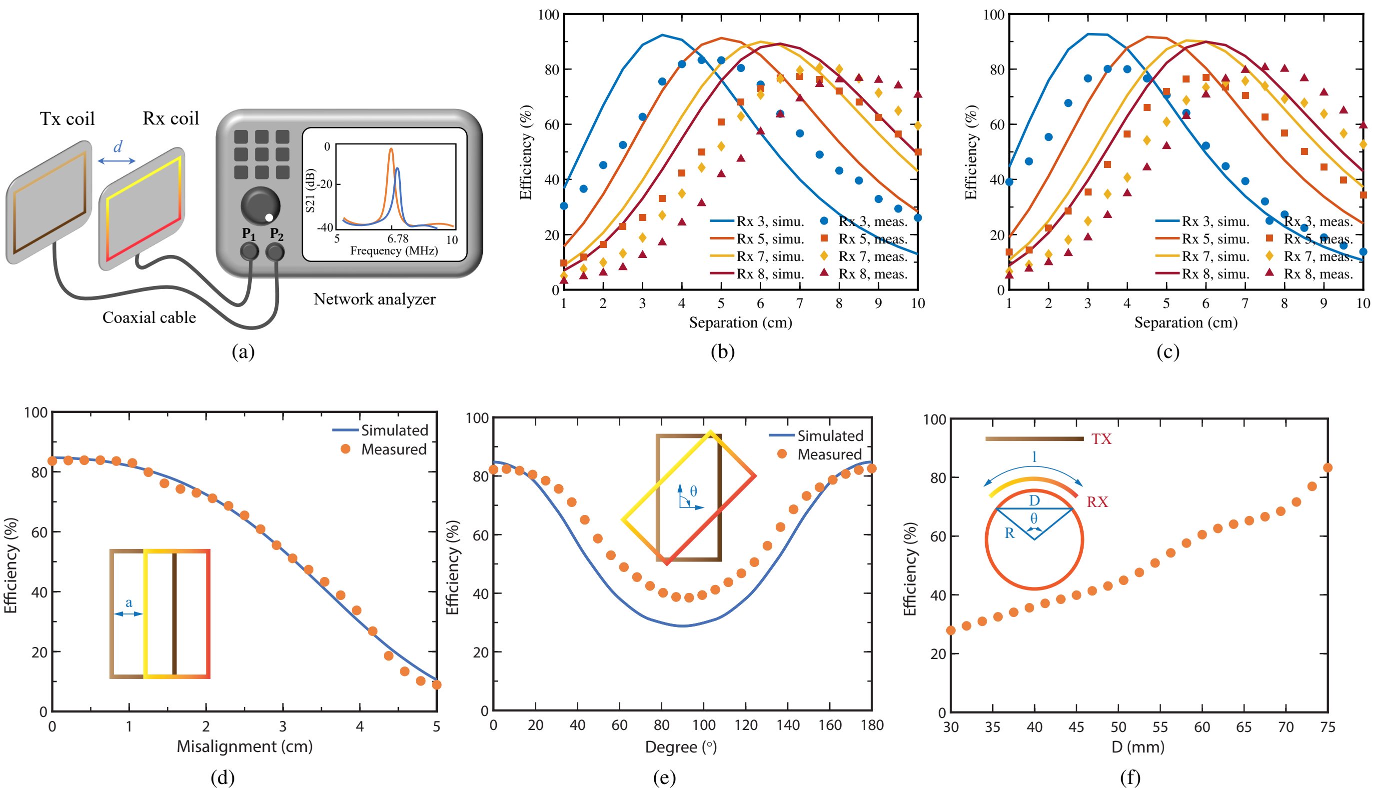

Fig. 9: (a) Experimental set-up measuring transmission coefficient, S_{21}, between the transmitter and receiver coils for various separation distance d. (b) measured WPT efficiency between the transmitter coil of 8 turns and receiver coil from 3 to 8 turns; (c) Transmitter coil of 7 turns and receiver coil from 3 to 8 turns at $6.78\,\mathrm{MHz}$; (d) Lateral; (d) Rotation; (e) Misalignment; (f) Bending misalignment measurements for coupling distance of $4.5\,\mathrm{cm}$ at $6.78\,\mathrm{MHz}$.

$d > 5\,\mathrm{cm}$. In the second experiment, the transmitting coil was replaced with the 7 turns coil and measured the efficiency of the system again. It can be noted that at an operating distance of $3.5\,\mathrm{cm}$, the measured WPT efficiency of the Rx coil of 3 turns is about 80% in free space, Fig. 9c. When $d < 3\,\mathrm{cm}$, the WPT efficiency falls due to the frequency splitting phenomena when the two coils are in close proximity, resulting in lower transfer efficiency at $6.78\,\mathrm{MHz}$. The frequency splitting relates to the increasing mutual inductance which causes a phase shift between the input voltage and the current, reducing the transferred power for the transmitting coil [68]. The simulated power efficiency is slightly higher than the measured power efficiency which is caused by the power lost to the parasitic resistance in the resonant capacitors. Additionally, discrepancies between the simulated and actual conductivity of Litz wire, and the differences between the simulated and fabricated coil dimensions, can lead to inaccuracies in the measured results. Fig. 9b and 9c that increasing the number of turns of the coil does not improve the WPT efficiency as additional turns can also lead to increased resistance and self-inductance. Therefore, for the proposed bandage design, we have selected Tx of 8 turns and Rx of 3 turns coil designs for designing the smart bandage system, thereby minimizing the overall area on the bandage occupied by the coil.

C. Misalignment Measurements

An important consideration in the practical implementation of WPT is the impact of misalignment between the transmitting and receiving coils. The power efficiency of the coils was studied under three misalignment conditions at a fixed coupling distance of $4.5\,\mathrm{cm}$: (i) lateral, (ii) rotational and (iii) bending misalignment. Fig. 9b illustrates that the measured power transfer efficiency of the system peaks at a coupling distance of 4.5 cm. Therefore, we selected this distance for the misalignment measurements. Fig. 9d shows the power efficiency against lateral misalignment distance a varying from 0 (aligned) to $5\,\mathrm{cm}$. As a increases, the strength of the magnetic field gradually decreases, and as a result, the power efficiency of the system decreases. When a = $5\,\mathrm{cm}$, the efficiency of the system has fallen to 10%. Fig. 9e shows the power efficiency against rotational misalignment varying from perfectly aligned at 0° and 180°, and 90° where the coils are orthogonal. The efficiency of the system drops to 40% when the coils are at 90°. This is due to reduced coupling between the coils and increased impedance in the circuit. Finally, the receiver coil was attached to a flexible plastic sheet which was used to form defined bending as shown in the inset of Fig. 9f and where D is the width of the coil given by:

$$D = 2Rsin\left(\frac{\theta}{2}\right) \tag{5}$$

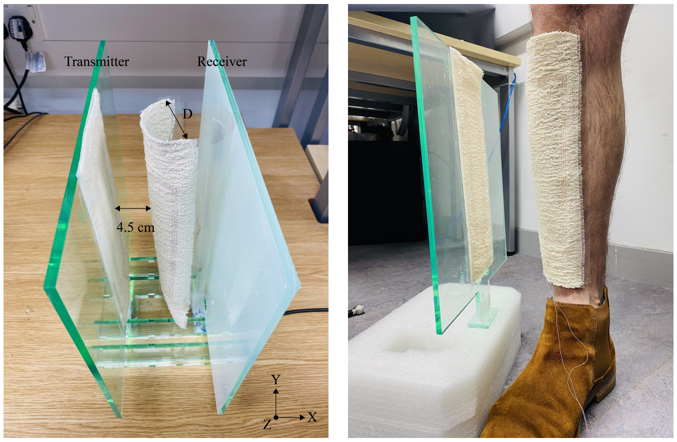

(a) (b)

Fig. 10: Measurement setup: (a) Bending misalignment of the receiver coil; (b) Receiver coil bent on the body.

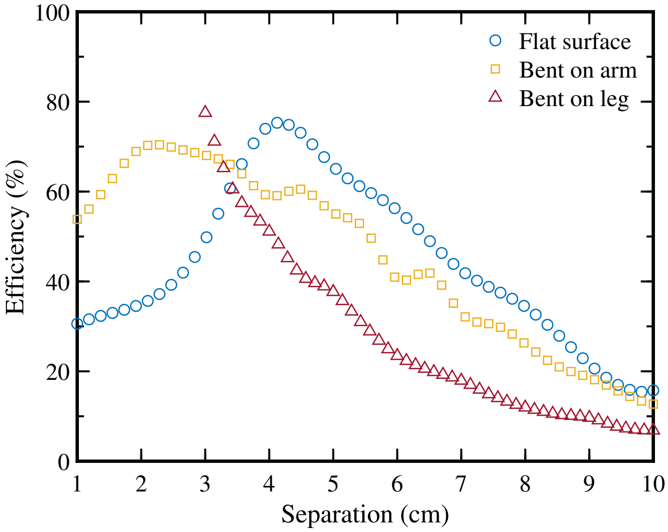

Fig. 11: WPT efficiency ($|S_{21}|^2$) measurements between the transmitter coil of 8 turns and receiver coil of 3 turns on the body at $6.78\,\mathrm{MHz}$.

where R is the radius of the circle, and θ is the central angle formed by the radii to the ends of the coil. The transmitter and receiver were $4.5\,\mathrm{cm}$ apart, and the receiver coil was bent around the y-axis, as shown in Fig. 10a. A larger D indicates a flatter receiver coil and as D decreases (i.e., the coil bends more) the transmission efficiency falls down to around 30% (Fig. 9f).

Several demonstrations of ergonomic wireless charging circuits that are more tolerant to misalignment have been reported [69]. Moreover, the metamaterials [70], or magneto-inductive waveguides [71], can be integrated into clothing to increase the collection area and allow the electromagnetic fields to be safely (within the SAR limits) coupled to the bandage.

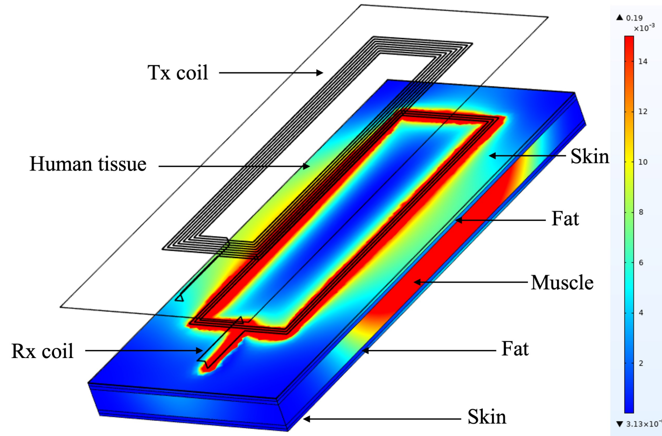

Fig. 12: Simulated SAR value of the WPT system at $6.78\,\mathrm{MHz}$.

TABLE II: Layered human model electrical parameters at $6.78\,\mathrm{MHz}$, [72].

	Density (kg/m^3)	Relative permittivity	Electrical conductivity (S/m)
Skin	1109	4.78E+2	1.47E-1
Fat	911	3.50E+1	4.96E-2
Muscle	1090	6.02E-1	2.33E+2

D. On-body Measurements

Fig. 11 depicts the measured power efficiency of the bandage system in the presence of the human body. The receiver coil was tested in three different configurations: on a flat body tissue, bent around a human arm (circumference $90\,\mathrm{mm}$) and finally a human leg (circumference $120\,\mathrm{mm}$), as shown in 10b. The result shows that the efficiency of the system was reduced to 75% at the same coupling distance of $3\,\mathrm{cm}$. The effect of bending on the achievable efficiency was also tested since the coils will be bent around the body. The results show that the efficiency of the system decreased to 60% at the same coupling distance of $4.5\,\mathrm{cm}$. The reduction in power efficiency is due to the change in resonance frequency and the decrease in the effective area of the receiving coil.

The specific absorption rate (SAR) in the human tissue was calculated in Comsol Multiphysics [73], Fig. 12, as follows:

$$E_{SAR} = \sigma \left(\frac{|E|^2}{\rho} \right) \tag{6}$$

where σ is the conductivity of the human tissue, ρ is the density, and E is the norm of the electric field (RMS). The human tissue consists of $1\,\mathrm{mm}$-thick skin and $10\,\mathrm{mm}$-thick fat, and $15\,\mathrm{mm}$-thick muscle was designed, shown in Fig. 12. Table II summarizes the electrical parameters of the human model. The Rx coil of 3 turns was mounted on the tissue and the SAR value simulated for separation distances of $1\,\mathrm{cm}$, $4.5\,\mathrm{cm}$ and $8\,\mathrm{cm}$ at a reference power of $1\,\mathrm{W}$. The results show that the SAR values are 0.004, 0.021 and 0.01 for

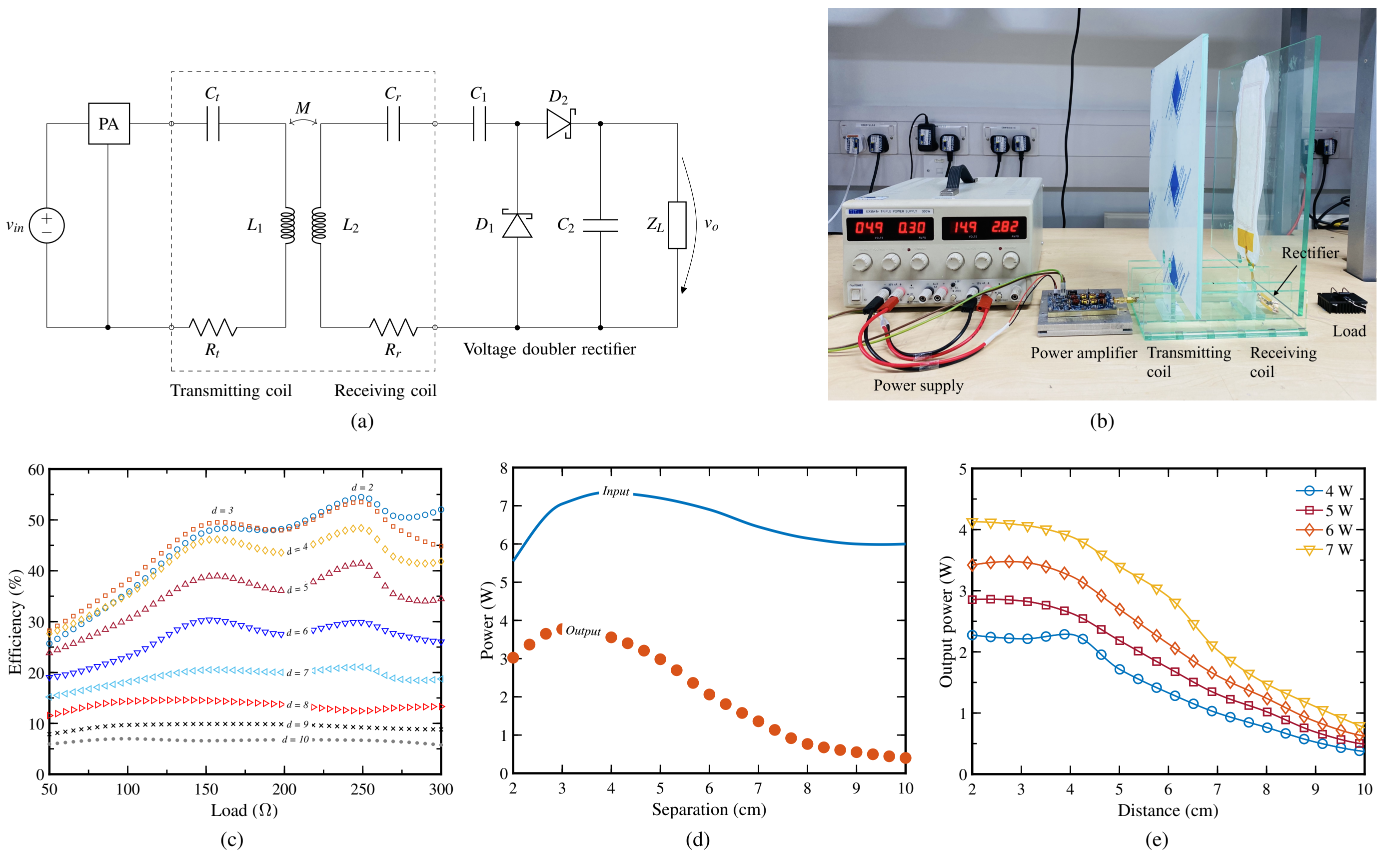

Fig. 13: (a) Equivalent circuit model representation of the WPT system; (b) Measurement set up for measuring the end-to-end efficiency against different load impedance at distance d in cm; (c) Measured end-to-end efficiency against different load impedance for various coupling distance; (d) Comparison between input and output power for optimal load impedance of $250\,\Omega$ at $6.78\,\mathrm{MHz}$; (e) Measured output power against different coupling distance from 2 to 10 cm for fixed input power from 4 to 7 W for optimal load impedance of $250\,\Omega$.

TABLE III:

Reference	This work	[84]	[85]	[86]
Power transfer method	Magnetic resonance coupling	Magnetic resonance coupling	Magnetic field resonance	Inductive coupling
Antenna type	Rectangular coil	Square spiral coil	Rectangular coil	Circular-spiral flat coil
Conductive material	Litz wire	Silver filament	Copper trace	Conductive past
Frequency	6.78 MHz	6.78 MHz	100 KHz	17.6 MHz
RX coil size	20×6.5 cm	8×12 cm	5.45×1.6 cm	14×14 cm
Transfer distance	10 cm	15 cm	n/a	10 mm
DC output power	4.1 W	24 mW	1.4 W	1.2 W
End-to-end efficiency	53.5%	46.2%	30%	37%

coupling distances of $1\,\mathrm{cm}$, $4.5\,\mathrm{cm}$, and $8\,\mathrm{cm}$, respectively. This suggests that the peak SAR is well below the 1.6 W/kg limit for wireless power transfer.

E. End-to-end Efficiency versus Load Impedance

The end-to-end efficiency of the system was investigated for different load impedances ranging from 50 to $300\,\Omega$. Fig. 13a shows the equivalent circuit model of the energy system, where v_{in} is a power source, *PA* is the power amplifier, C_t and R_t are the capacitance and resistance of the transmitting coil, respectively, C_r and R_r represent the capacitance and resistance of the receiver coil, respectively, and Z_L is the load impedance. L_1 and L_2 are the inductance of the transmitting and receiving coil, respectively, and M is the mutual inductance between the coupling coils. A voltage doubler rectifier was employed between the receiver and the load. The measurement setup for measuring end-to-end efficiency is shown in Fig. 13b. A dc power supply was used to power the amplifier. The output voltage of the power supply was set to $15\,\mathrm{V}$. The transmitter was connected to an RF power amplifier. The power amplifier, *GSWP050W-EVBPA* from GaN systems [74], is a $50\,\mathrm{W}$, $6.78\,\mathrm{MHz}$ Class EF2 power amplifier designed for wireless power transfer. The receiver was connected to a voltage doubler rectifier (Fig. 6). The variable resistive load (non-inductive) was connected at the rectifier output, and the voltage across the load was monitored with an oscilloscope. The load was mounted on a heat sink to reduce the heat of

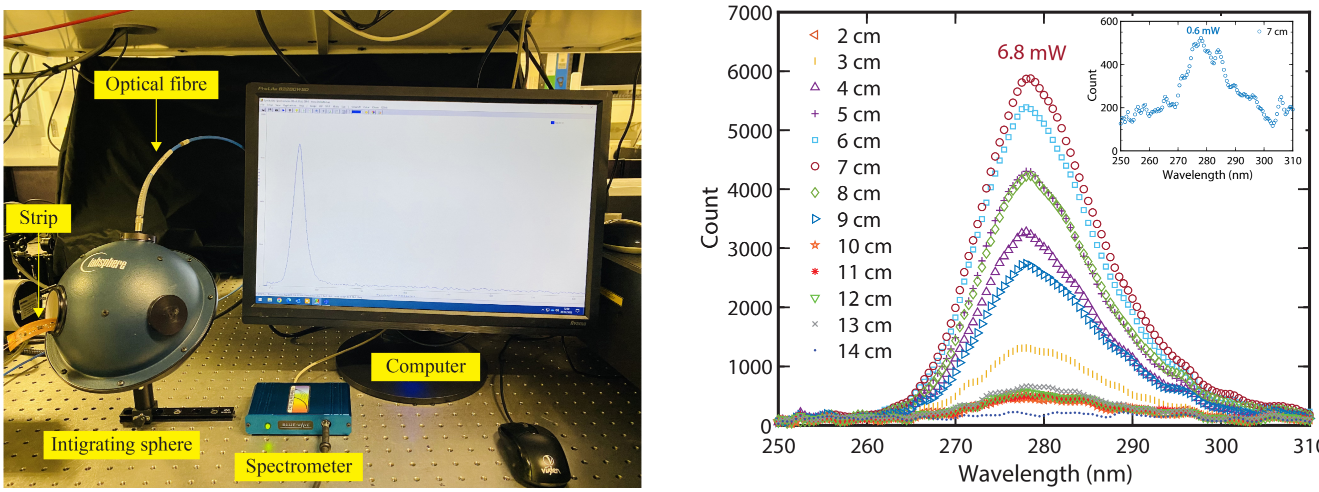

(a) (b)

Fig. 14: (a) Measurement setup for measuring the optical performance of the LEDs strip; (b) Measured radiated power of LEDs strip for at distance d from 2 to $14\,\mathrm{cm}$ at an integration time of $500\,\mathrm{ms}$.

the resistor. The separation distance between the coupling coils varied from 2 to $10\,\mathrm{cm}$.

Fig. 13c shows the measured transmission efficiency of the WPT system for different load impedance Z_L at separation distances d ranging from 2 to $10\,\mathrm{cm}$ at $6.78\,\mathrm{MHz}$. It can be observed that the system has a high end-to-end efficiency of over 50% for the optimal load impedance of $250\,\Omega$ when $d < 3\,\mathrm{cm}$. As the separation increases, the efficiency decreases. When $d = 10\,\mathrm{cm}$, the efficiency of the system dropped to below 10%. At separation distances of $7\,\mathrm{cm}$ or less, the efficiency decreases as the load impedance decreases below $250\,\Omega$. The load resistance has little effect of distances of $8\,\mathrm{cm}$ or more. A comparison between the input and output power versus d for an optimal load impedance of $250\,\Omega$ is illustrated in Fig. 13d. This shows the output power is maximum when d is $3\,\mathrm{cm}$ at $6.78\,\mathrm{MHz}$.

Furthermore, measurements were carried out to examine the output power of the system at fixed input power levels of $4\,\mathrm{W}$, $5\,\mathrm{W}$, $6\,\mathrm{W}$, and $7\,\mathrm{W}$ for optimal load impedance $250\,\Omega$, as shown in Fig. 13e. The system provides approximately $2.25\,\mathrm{W}$ for an input power of $4\,\mathrm{W}$ at coupling distances between $2\,\mathrm{cm}$ and $4\,\mathrm{cm}$. Beyond $4\,\mathrm{cm}$ coupling distance, the output power of the system starts to decrease. As input power increases, the output power of the system increases, as expected. Based on these measurements, it can be inferred that the LED strip can be activated at a coupling distance of $10\,\mathrm{cm}$ with an input power of $5\,\mathrm{W}$ since the LED strip consumes approximately $0.55\,\mathrm{W}$ of power. Table III presents a comparison of the proposed wireless system with existing fabric and flexible WPT systems, demonstrating that the proposed system can transfer a high power of $4.1\,\mathrm{W}$ with an end-to-end efficiency of 53.5%. It can be noted that a power of $4.1\,\mathrm{W}$ is not required to operate the proposed anti-infective smart bandage. These measurements demonstrate the end-to-end efficiency of the system and suggest that such high-power transfer is possible with all fabric bandage coils. Nevertheless, the input power can be easily adjusted in the power supply for low-power devices.

F. Light Emission Measurement

The measurement setup shown in Fig. 14a was used to investigate the optical performance of the UVC LEDs in two states: (i) LED strip without a bandage and (ii) LED strip assembled in a fabric bandage. The LED strip was placed inside a calibrated integrating sphere which provides uniform scattering and collects all the light from the UVC source. The integrating sphere was connected to a SpectraWiz spectrometer via optical fibre. The power emission from the LEDs was measured for coupling distances d from 1 to $14\,\mathrm{cm}$. Fig. 14b shows the radiant power emission of the LEDs when they were wirelessly powered, showing that at $7\,\mathrm{cm}$, the LEDs radiate the highest power. The level of light emission drops significantly when the receiver coil was in close proximity to the transmitter coil (e.g. $2\,\mathrm{cm}$ and $3\,\mathrm{cm}$) or at larger distances in excess of $9\,\mathrm{cm}$. The peak power emission at $7\,\mathrm{cm}$ is due to the impedance matching between the LEDs strip and the receiver coil. The radiant power of the LED strip decreases when the receiver and transmitter coils are in close proximity, this is attributed to the effect of frequency splitting at distances below 3 cm. As the separation distance between the coils increased to 9 cm, the efficiency gradually decreased due to the weakening of the magnetic field strength with distance. When the circuit is assembled in the fabric bandage, the radiated power of the LEDs has significantly degraded as shown in the inset of Fig. 14b. This is due to the absorption of the UV radiation by the textile fibres [75]. Here the optical system count has been converted to mW using data sheet values from [76] for the typical LED radiant power of $3\,\mathrm{mW}$ and $4.3\,\mathrm{mW}$ at $20\,\mathrm{mA}$ and $30\,\mathrm{mA}$, respectively. For an output radiant power of $3\,\mathrm{mW}$, the number of counts was 2650 at $277\,\mathrm{nm}$. Similarly, for an output radiant power of $4.3\,\mathrm{mW}$, the

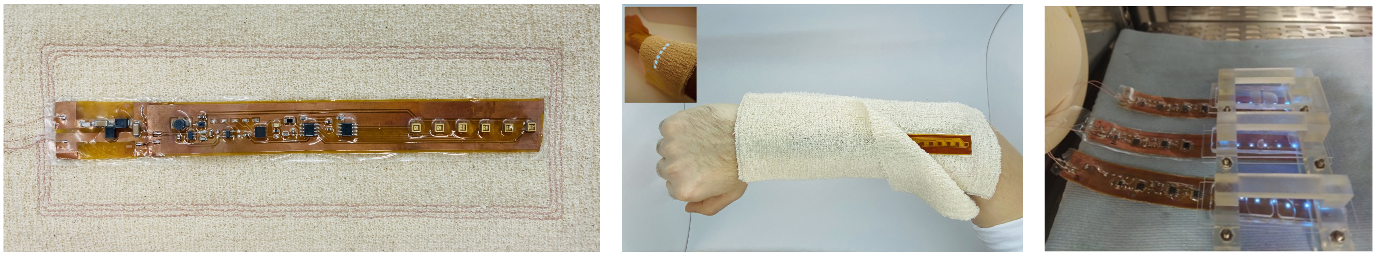

(a) (b) (c)

Fig. 15: (a) Final prototype of the anti-infective smart bandage; (b) Mounted on the body (the LEDs strip should face the site of the wound when in use); (c) Experimental setup with the UVC LEDs without bandage in $4\,\mathrm{cm}$ distance.

number of counts was 3645 at $277\,\mathrm{nm}$. These two reference values can be extrapolated for the conversion. Furthermore, an input power of $4.32\,\mathrm{W}$ at a coupling distance of $7\,\mathrm{cm}$ is required to achieve high radiant power of $6.8\,\mathrm{mW}$. The bandage consumes approximately $0.55\,\mathrm{W}$ of power, resulting in a power transfer efficiency of 12.73%. Fig. 15a shows the final prototype of the anti-infective smart bandage and Fig. 15b illustrates the bandage mounted on the body. The UVC LEDs have the ability to emit 100% radiant intensity at a wide angle of 80° face up. Additionally, the wound dressing used to enclose the strip will also act as a light diffuser to further disseminate the UVC light emission, as shown in the inset of Fig 15b. Further uniform emission can be achieved by reducing the gap between the UVC LEDs and increasing the thickness of the wound dressing due to its wide radiating angle of 80°. Furthermore, the number of LEDs in the bandage system can be easily increased as the proposed WPT system harvests enough power to operate them. Literature reports that the intensity of the UVC emission will not largely affect the performance of inactivating microorganisms. Extending the time or increasing the intensity will improve the performance by log-reduction [77], by disturbing their DNA replication via crosslinking between thymine and cytosine in the same DNA strand.

IV. Anti-bacterial Properties

A. Bacterial Strain and Growth Condition

Marine bacteria belonging to the genus *Pseudoalteromonas* are known to produce numerous compounds of biotechnological interest [78]. In this study, we used *Pseudoalteromonas* sp. D41 strain which is a Gram-negative bacteria and was isolated from Brest Bay (Brittany, France). Gram-negative bacteria are associated with infections in the bloodstream and in wounds or surgical sites and are becoming increasingly resistant to most available antibiotics [79]. *Pseudoalteromonas* sp. D41 bacteria has been mainly studied for its exceptionally strong adhesion properties on a wide range of substrates [80]–[83] and was grown in Marine Broth 2216 (MB) culture media at ambient temperature under aerobic conditions with continuous agitation overnight. The optical density (OD) of the suspension was defined at $600\,\mathrm{nm}$ with a Jenway 6400 UV-VIS spectrophotometer. The final OD of the cell culture media was set to OD 0.2 in MB culture media.

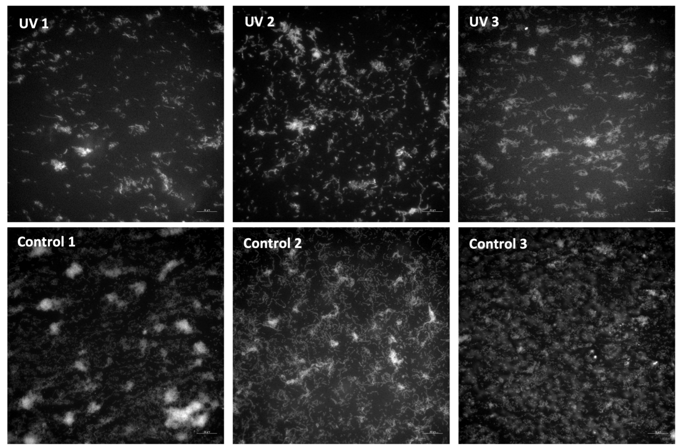

Fig. 16: Biofilm formation after six-hour long UVC radiation at $19\,^{\circ}\mathrm{C}$. UV 1 corresponds to the UVC LED Sample 1, UV 2 to the UVC LED Sample 2 and UV 3 to the UVC LED Sample 3. Control samples were incubated under the same conditions without UVC light. The initial cell concentration was OD 0.2 in MB culture media. Images were taken with 63 X magnification using a Zeiss Imager Z2 microscope equipped with the Apotome.2 sliding module.

B. Experimental Setup for UV Illumination

UVC radiation was applied to *Pseudoalteromonas* sp. D41 bacteria in the MB culture media. The setup, including a power supply and sample holder, was designed and manufactured in-house using a Form3 (Formlabs®) 3D printer, as shown in Fig. 15c. One millilitre of the bacteria cell culture (OD 0.2) was pipetted into $1.3\,\mathrm{mL}$ PDMS chambers, cast from 3 printed molds. This arrangement provided aerobic conditions for the cells. The PDMS chambers were closed with quartz glass slides using 3D printed clips preventing any leakage of the culture media out of the chambers. The samples were then turned over so that the quartz glass slides were placed on the bottom to better observe biofilm formation on their surface. The cells were radiated with the UVC LEDs from below for six hours at $19\,^{\circ}\mathrm{C}$. The temperature of the cells was tested before and after the experiments using a C.A 1954 DiaCAM thermal imaging IR camera and no considerable heating effect was observed.

Three different light intensities were tested, UV sample 1

TABLE IV: Cell growth after six hours of UVC radiation at 19 °C with and without bandage, in one and four centimetres distance. The initial cell concentration was OD 0.2 in MB culture media.

	$No\ UV$		$UV1-275\ nm$		$UV2-275\ nm$		$UV3-268\ nm$	
	OD^{a}_{Final}	CG^{b}	OD_{Final}	CG	OD_{Final}	CG	OD_{Final}	CG
$No\ bandage, 1\ cm$	0.66	3.3X	0.15	0.8X	0.13	0.7X	0.15	0.8X
$Bandage, 1\ cm$	0.6	3X	0.14	0.7X	0.2	1X	0.18	0.9X
$Bandage, 4\ cm$	0.71	3.5X	0.11	0.6X	0.22	1X	0.16	0.8X

[a]Optical Density, [b]Cell Growth

~250 µW where the UVC LEDs were not covered with fabric bandage and the illumination distance was 1 cm, UV sample 2 ~25–40 µW where the UVC LEDs were covered with fabric bandage and the illumination distance was 1 cm, and UV sample 3 with less than 10 µW where the UVC LEDs were covered with fabric bandage and the illumination distance was 4 cm. All conditions were tested three times: As references, two chambers of cell culture media and one control sample of MB culture media were always incubated in parallel without UVC radiation.

C. Biofilm Observation

Biofilms developed on the quartz glass slides were rinsed with artificial sea water (ASW) and then fixed in 2.5% formaldehyde in ASW at room temperature for 30 min. After rinsing with ASW; 1:1 ASW, milliQ water and finally with milliQ water, the slides were dried and mounted with SlowFade™ Gold antifade reagent with DAPI (Invitrogen). Biofilm observation was carried out using an Olympus BX fluorescent microscope and a Zeiss Imager Z2 microscope equipped with the Apotome.2 sliding authmodule, as shown in Fig. 16.

D. Discussion

Fig. 16 shows that after being exposed to UV light, three different effects were observed on the bacterial cells: (i) the cell growth slowed down or immediately stopped, (ii) morphological changes appeared on the cells, (iii) biofilm formation was less efficient resulting in lower surface coverage. Cell growth was calculated by measuring the OD of the supernatant before and after UVC radiation, as summarized in Table IV. Control samples, not exposed to UVC, had a final cell concentration of approximately 0.6 OD after a six-hour incubation at 19 °C. The cell concentration was thus three times higher than the initial cell concentration of OD 0.2. After the application of UVC LED, the cells stopped growing and a constant or lower final OD was measured at the end of the experiments. This is due to the morphological changes the cells went through as a result of the UVC irradiation. UV light harms cells by directly damaging the DNA and therefore causing cell apoptosis. This process resulted in a considerable, twofold decrease of cell size, from 3–4 µm to 1–2 µm.

After few hours, biofilms start to develop on the glass slides. The surface was covered with bacteria cells in 27% (±6%) with UVC radiation independently from the intensity of the UVC light. Control samples without UVC radiation showed 60% (±30%) coverage with multi-layered cell depositions in some places.

UVC LEDs were shown to have a considerable effect on cell growth independently from the applied light intensity, no big difference was observed in between the UVC LEDs of 250 µW, 25–40 µW and less than 10 µW. This very low light intensity of 10 µW was enough to cause immediate cell apoptosis, disrupt cell growth and reduce biofilm formation. The cellular surface coverage was less than half of the coverage of the control samples. Table V compares the proposed anti-infective smart bandage and the state-of-the-art, demonstrating the first wirelessly powered therapeutic smart bandage for chronic wound care and management.

The proposed wireless system has the advantage of being sustainable and having a better form-factor than disposable batteries. For instance, the bandage presented in [89] uses a rigid battery that is 30 mm × 45 mm, making it bulky and heavy for the user. Since UV treatment must be applied for several hours, multiple batteries will be needed for a single treatment session, which makes it impossible to use the system while the patient is sleeping or without dedicated personnel. Rechargeable batteries also pose a risk to the user as they cannot be encapsulated, and they may come in contact with fluids or other conductors, which could cause a sudden temperature rise.

V. Conclusion

In this paper, a novel drug-free and anti-infective smart bandage for treating chronic non-healing wounds is demonstrated. The proposed bandage is battery-free and powered by a 6.78 MHz wireless power transfer. Despite being partially obscured by the fabric bandage, the low-power UVC LEDs have been shown to effectively eradicate bacteria at low radiant power levels. It was found that polyimide coating completely blocks UV transmission. The low levels of radiated power minimize the risks of the radiation being harmful to the human eyes and if required then polyurethane film could be added to the bandage to prevent leakage. Flexible transmitter and receiver coils were successfully fabricated on a standard bandage fabric and achieved efficient and effective wireless power transfer. The specific dimensions of the coils, 200 mm × 65 mm, may be not optimal for all wound types and sizes. It may be necessary to adjust the size of the coils, the distance

TABLE V: Comparison of the proposed anti-infective smart bandage and the state-of-the-art.

Reference	Sensing and drug delivery mechanism	Target Bacteria and Treatment	Power supply	Bandage integration	Advantages	Disadvantages
This work	User-activated passive drug delivery	•Bacteria: Pseudoalteromonas sp. D41 •*Treatment:* UVC radiation	Magnetic resonance wireless power transfer	A polyurethane encapsulated flexible UVC strip is seamlessly embedded within a cotton crepe bandage	•Completely avoids bacterial resistance during treatment. •Radiation time and dosage control using integrated MCUs. •Electronics can be reused when the dressing is changed. •Autonomous and battery-less power supply for the bandage for up to 10 cm separation distance between receiver and transmitter coils.	•Would benefit from the integration of sensors for biomarker tracking and real-time wound monitoring for activation of UVC radiation. •UVC radiation time can range from 30 mins to 6 hours depending on the number of UVC LEDs and the size of the wound and the severity of the infection.
[87]	Wound temperature, pH and uric acid monitoring and heater activated drug delivery	•Bacteria: Staphylococcus aureus •*Treatment:* Antibiotics (cefazolin)	NFC	PDMS encapsulated flexible circuit on is glued on a transparent film (Tegaderm film, 3M) dressing	•Sensor activated delivery of antibiotics and capability to monitor multiple parameters influencing wound healing. •Dosage control of antibiotics delivery. •Bandage is battery-free and uses near field wireless power supply in very close proximity. The exact range is not reported.	•Prone to antibiotic resistance. •Encapsulated antibiotics can be limited in quantity for continuous treatment of chronic wounds. •Integrated bacterial treatment is not reusable when the bandage needs to be replaced due to large exudate absorption from wounds.
[88]	Reaction based monitoring of wound pH, glucose and temperature level to activate drug delivery with an active antibacterial polymer	•Bacteria: Gram-negative (Escherichia coli) and Gram-positive bacteria (Staphylococcus aureus) •*Treatment:* Antibacterial polymer (CTAB- cetyltrimethylammonium bromide)	None	PUIDE Elastomer	•Real-time monitoring of wound physiological state. •Eliminates the need for power supply.	•Antibacterial polymer contains CTAB (cetyltrimethylammonium bromide) which can be toxic to cells at high dosages and hence dosage control is critical. •Bandage is entirely reaction based, hence would treatment be not reusable or recyclable.
[89]	Temperature and pH sensors and thermally activated hydrogel drug dispenser via flexible microheater	•Bacteria: Staphylococcus aureus •*Treatment:* Antibiotics (cefazolin)	Battery powered from an electronic module	Antibacterial patch demonstrated on non-textile PET and Parylene films; and rigid PCB electronics to drive bandage film	•Capability for real-time multi-parameter wound monitoring for healing management. •Sensor activated controlled delivery of antibiotics to the wound.	•Smart bandage is not battery-free and required a rigid module which can make usage uncomfortable. •Increased power consumption as integrated heater requires an activation temperature ($42\,^{\circ}$C) for 30 mins to activate drug delivery.
[90]	Temperature sensor and in-situ UV-responsive antibacterial hydrogel	•Bacteria: Staphylococcus aureus •*Treatment:* Antibiotics (Gentamicin)	External battery	PDMS encapsulated flexible PCB and hydrogel	•Capability for wound temperature monitoring and Bluetooth data transfer for real-time wound management. •Low UV activation period for antibiotic release (1 to 5 mins). •Integrated flexible electronics is encapsulated with biocompatible PDMS. •Flexible electronics showed good fatigue resistance to a maximum tensile strain of 6% for 20 cycles.	•Bandage still requires the use of an external battery for UV activation and temperature monitoring. •Bandage is not effective for antibiotic resistant bacterial infections.
[91]	Photothermal zwitterionic microneedle coated with ZnO nanoparticles for drug delivery	•Bacteria: Staphylococcus aureus and Escherichia coli •*Treatment:* Zinc oxide (ZnO) nanoparticles and Asiaticoside	None	zwitterionic polymer polysulfobetaine methacrylate (PSBMA) and hydrogel	•Treatment is effective against drug-resistant bacteria. •High penetration depth of applied antibacterial to the wound.	•Bandage treatment is one-time use and would require. •Dosage control of applied antibacterial agent is not reported. •No wound sensing mechanism.

between the Tx and Rx coils and the transmission performance of the system to optimize the system for different wound types. The UV-emitting bandage offers a wound management approach that can reduce the use of antibiotics. A flexible rectifier based on voltage doubler topology which delivers peak output DC voltage was designed. The rectifier has an RF-to-DC efficiency of 91% and can deliver a power transfer of 4.1 W which is significantly higher when compared to the rectifier proposed in [84].

The bandage system has a DC-to-DC converter that limits the maximum current delivered to the load. The converter reduces its output voltage when the load current exceeds the current limit to prevent further increase and protect the converter and load. The flexible circuit strip is isolated by a polyimide film to ensure the user is never in contact with the active traces, minimizing the risk of electric shocks to the human body. In terms of electromagnetic (EM) safety, the SAR simulations show that the system can operate at its maximum RF input level (exceeding 10 W) while staying under 50% of the maximum SAR level of 1.6 W/kg.

The treatment duration for chronic wounds using UVC LED-embedded bandages will depend on several factors, including the size and severity of the wound. Generally, the bandage can be used for a specific duration ranging from 30 min to a few hours to ensure effective treatment. The bandage does not necessarily have to radiate continuously for 6 hours to treat the wound. In the anti-bacterial properties measurements, the irradiation period of 6 hours was chosen to quantify the effect of UV LED radiation on the formation of the bacterial biofilm [92]. The transmitter coil, at a coupling distance of 7 cm, provides optimal power to the bandage for treating bacteria. The flexible electronic circuit implementation allows straightforward future expansion to integrate sensors, enabling the smart bandage to perform real-time monitoring (including any risk of reinfection) as well as to treat infected and persistent wounds. The development of the fabric bandage to diffuse the light over a wider area will also enable UV LEDs to cover a wider area with the potential to reduce the number of LEDs required and hence the size and complexity of the electronics.

Acknowledgment

We thank Jeff Hooker for helping with mounting components on the circuits.

References

[1] R. G. Frykberg and J. Banks, "Challenges in the treatment of chronic wounds," *Adv. Wound Care (New Rochelle)*, vol. 4, no. 9, pp. 560–582, 2015.

[2] W. Alam, J. Hasson and M. Reed, "Clinical approach to chronic wound management in older adults," *J. Am. Greiatr. Soc.*, vol. 69, pp. 2327–2334, 2021.

[3] K. Jarbrink, et al., "The humanistic and economic burden of chronic wounds: a protocol for a systematic review," *Syst. Rev.*, vol. 6, no. 1, 2017.

[4] InformedHealth.org [Internet]. Cologne, Germany: Institute for Quality and Efficiency in Health Care (IQWiG); 2006-. What are the treatment options for chronic wounds? Oct. 17 2006, [Updated 2018 Jun. 14].

[5] R. G. Frykberg and J. Banks, "Challenges in the treatment of chronic wounds," *Adv. Wound Car.*, vol. 4, no. 9, pp. 560–582, 2015.

[6] J. G. Powers, C. Higham, K. Broussard, T. J. Phillips, "Wound healing and treating wounds: Chronic wound care and management," *J. Am. Acad. Dermatol.*, vol. 74, no. 4, pp. 607–625, 2016.

[7] J. Linfors, "A comparison of an antimicrobial wound cleanser to normal saline in reduction of bioburden and its effect on wound healing," *Ostomy/wound management,* vol. 50, no. 8, pp. 28–41, 2004.

[8] M. Farahani and A. Shafiee, "Wound healing: From passive to smart dressings," *Adv. Healthc. Mater.*, vol. 10, no. 16, p. 2100477, 2021.

[9] P. Mostafalu et al., "Smart bandage for monitoring and treatment of chronic wounds," *Small*, vol. 14, no. 33, p. 1703509, 2018.

[10] R. Dong and B. Guo, "Smart wound dressings for wound healing," Nano Today, vol. 41, p. 101290, 2021.

[11] C. Wang, S. S. Ehsan and G. Wei, "Wearable bioelectronics for chronic wound management," *Adv. Funct. Mater.*, vol. 32, no. 17, p. 2111022, 2022.

[12] T. Juknius et al., "Antimicrobial properties of diamond-like carbon/silver nanocomposite thin films deposited on textiles: towards smart bandages," *Materials*, vol. 9, no. 5, p. 371, 2016.

[13] A. Lumbreras-Aguayo et al., "Poly (methacrylic acid)-modified medical cotton gauzes with antimicrobial and drug delivery properties for their use as wound dressings," *Carbohydrate polymers*, vol. 205, pp. 203–210, 2019.

[14] G. Rivero, M. Meuter, A. Pepe, M. Guevara, A. R. Boccaccini and G. A. Abraham, "Nanofibrous membranes as smart wound dressings that release antibiotics when an injury is infected," *Colloids and Surf. A Physicochem. Eng. Asp.*, vol. 587, pp. 124313, 2020.

[15] O. Alaysuy et al., "Development of green and sustainable smart biochromic and therapeutic bandage using red cabbage (Brassica oleracea L. Var. capitata) extract encapsulated into alginate nanoparticles," *Int. J. Biol. Macromol.*, vol. 211, pp. 390–399, 2022.

[16] Q. Pang, L. Dong, L. Shijian, W. Guangming, Q. Bianbian, D. Shurong, M. Lie, G. Changyou and W. Zhaohui, "Smart flexible electronics-integrated wound dressing for real-time monitoring and on-demand treatment of infected wounds," *Adv. Science*, vol. 7, no. 6, p. 1902673, 2020.

[17] H. Lee et al., "A graphene-based electrochemical device with thermoresponsive microneedles for diabetes monitoring and therapy." *Nature Nanotech.*, vol. 11, no. 6, pp. 566–572, 2016.

[18] T. Dai, M. S. Vrahas, C. K. Murray and M. R. Hamblin, "Ultrviolet C irradiation: an alternative antimicrobial approach to localized infections?" *Expert Rev. Anti Infect. Ther.*, vol. 10, no. 2, pp. 185–195, 2012.

[19] N. Yeh, T. J. Ding and P. Yeh, "Light-emitting diodes light qualities and their corresponding scientific applications," *Renewable and Sustainable Energy Rev.*, vol. 51, pp. 55–61, 2015.

[20] L. M. Hinds, C. P. O'Donnell, M. Akhter and B. K. Tiwari, "Principles and mechanisms of ultraviolet light emitting diode technology for food industry applications," *Innov. Food Sci. Emerg. Technol.*, vol. 56, p. 102153, Aug. 2019.

[21] K. Song, F. Taghipour and M. Mohseni, "Microorganisms inactivation by wavelength combinations of ultraviolet light-emitting diodes (UV-LEDs)," *Sci. Total Environ.*, vol. 665, pp. 1103–1110, 2019.

[22] I. M. Caminiti, et al., "The effect of ultraviolet light on microbial inactivation and quality attributes of apple juice," *Food Bioprocess Technol.*, vol. 5, no. 1, pp. 680–686, Mar. 2012.

[23] S. K. Bhardwaj, et al., "UVC-based photoinactivation as an efficient tool to control the transmission of coronaviruses," *Sci. Total Environ.*, vol. 792, p. 148548, 2021.

[24] A. Gupta, P. Avci, T. Dai, Y. Y. Huang and M. R. Hamblin, "Ultraviolet radiation in wound care: sterilization and stimulation," *Adv. Wound Care (New Rochelle)*, vol. 2, no. 8, pp. 422–437, 11 Oct. 2013.

[25] J. C. Goh et al., "Disinfection capabilities of a 222 nm wavelength ultraviolet lighting device: a pilot study," *J. Wound Care*, vol. 30, no. 2, Feb. 2021.

[26] T. Dai, M. S. Vrahas, C. K. Murray and M. R. Hamblin, "Ultraviolet C irradiation: an alternative antimicrobial approach to localized infections?," *Taylor & Francis*, vol. 10, no. 2, pp. 185–195, Jan. 2012

[27] Y. Ou and P. M. Petersen, "Application of ultraviolet light sources for in vivo disinfection," *Jpn. J. Appl. Phys.,* vol. 60, no. 10, pp. 100501, 2021.

[28] J. Glaab, et al., "Skin tolerant inactivation of multiresistant pathogens using far-UVC LEDs," *Sci. Rep.*, vol. 11, no. 1, p. 14647, 19 Jul. 2021.

[29] M. R. Hamblin and H. Abrahamse, "Can light-based approaches overcome antimicrobial resistance?," *Drug Dev. Res.*, vol. 80, pp. 48–67, 2019.

[30] K. Narita, et al., "Disinfection and healing effects of 222-nm UVC light on methicillin-resistant Staphylococcus aureus infection in mouse wounds," *J. Photochem. Photobiol. B.*, vol. 178, pp. 10–18, Jan. 2018

[31] P. Mostafalu, W. Lenk, M. R. Dokmeci, B. Ziaie, A. Khademhosseini and S. R. Sonkusale, "Wireless flexible smart bandage for continuous monitoring of wound oxygenation," *IEEE Trans. Biomed. Circuits Syst.*, vol. 9, no. 5, pp. 670–677, Oct. 2015.

[32] H. Derakhshandeh, S. S. Kashaf, F. Aghabaglou, I. O. Ghanavati and A. Tamayol, "Smart bandages: the future of wound care," *Trends Biotechnol.*, vol. 36, no. 12, pp. 1259–1274, 2018.

[33] D. Vital, J. L. Volakis and S. Bhardwaj, "An ultra-high-frequency wirelessly-powered smart bandage for wound monitoring and sensing using frequency modulation," IEEE MTT-S Int. Microw. Symp. (IMS), 2021, pp. 331–334.

[34] F. Nikbakhtnasrabadi, E. S. Hosseini, S. Dervin, D. Shakthivel and R. Dahiya, "Smart bandage with inductor-capacitor resonant tank based printed wireless pressure sensor on electrospun poly-L-lactide nanofibers," *Adv. Electron. Mater.*, vol. 8, p. 2101348, 2022.

[35] M. Farooqui and A. Shamim, "Low cost inkjet printed smart bandage for wireless monitoring of chronic wounds," *Sci. Rep.*, vol. 6, p. 28949, 2016.

[36] P. Escobedo, M. Bhattacharjee, F. Nikbakhtnasrabadi and R. Dahiya, "Smart bandage with wireless strain and temperature sensors and batteryless NFC tag," *IEEE Internet of Things J.*, vol. 8, no. 6, pp. 5093–5100, 15 Mar. 2021.

[37] M. Wagih et al., "Microwave-enabled wearables: underpinning technologies, integration platforms, and next-generation roadmap," *IEEE J. Microwaves*, vol. 3, no. 1, pp. 193–226, Jan. 2023.

[38] G. Namgoong et al., "A 6.78 MHz, 95.0% peak efficiency monolithic two-dimensional calibrated active rectifier for wirelessly powered implantable biomedical devices," *IEEE Trans. Biomed. Circuits Syst.*, vol. 15, no. 3, pp. 509–521, June 2021.

[39] Y. Jia et al., "A Trimodal Wireless Implantable Neural Interface System-on-Chip," IEEE Trans. Biomed. Circuits Syst., vol. 14, no. 6, pp. 1207–1217, Dec. 2020.

[40] M. Wagih, A. Komolafe and B. Zaghari, "Dual-receiver wearable 6.78 MHz resonant inductive wireless power transfer glove using embroidered textile coils," *IEEE Access*, vol. 8, pp. 24630–24642, 2020.

[41] Z. Zhang, H. Pang, A. Georgiadis and C. Cecati, "Wireless power transfer—an overview," *IEEE Trans. Ind. Electron.*, vol. 66, no. 2, pp. 1044–1058, Feb. 2019.

[42] T. S. Pham, et al., "Optimal frequency for magnetic resonant wireless power transfer in conducting medium," *Sci. Rep.*, vol. 11, p. 18690, 2021.

[43] S. H. Kang, J. H. Choi, F. J. Harackiewicz and C. W. Jung, "Magnetic resonant three-coil WPT system between off/in-Body for remote energy harvest," *IEEE Microw. Wirel. Compon. Lett.*, vol. 26, no. 9, pp. 741–743, Sept. 2016.

[44] K. Bao, C. L. Zekios and S. V. Georgakopoulos, "A wearable WPT system on flexible substrates," *IEEE Antennas Wirel. Propag. Lett.*, vol. 18, no. 5, pp. 931–935, May 2019.

[45] M. Wagih, A. Komolafe, A. Weddell and S. Beeby, "1 μW–3.75 W dual-mode near/far-field wearable wireless power transfer using a hybrid rectenna", *2022 Wireless Power Week (WPW)*, pp. 298–301, 2022.

[46] I. Ortego-Isasa, K. P. Benli, F. Casado, J. I. Sancho and D. Valderas, "Topology analysis of wireless power transfer systems manufactured via inkjet printing technology," *IEEE Trans. Ind. Electron.*, vol. 64, no. 10, pp. 7749–7757, Oct. 2017.

[47] N. J. Grabham, Y. Li, L. R. Clare, B. H. Stark and S. P. Beeby, "Fabrication techniques for manufacturing flexible coils on textiles for inductive power transfer," *IEEE Sens. J.*, vol. 18, no. 6, pp. 2599–2606, 15 Mar. 2018.

[48] S. H. Kang and C. W. Jung, "Textile resonators with thin copper wire for wearable MR-WPT system," *IEEE Microw. Wirel. Compon. Lett.*, vol. 27, no. 1, pp. 91–93, Jan. 2017.

[49] G. Monti, L. Corchia and L. Tarricone, "UHF wearable rectenna on textile materials," *IEEE Trans. Antennas Propag.*, vol. 61, no. 7, pp. 3869–3873, Jul. 2013.

[50] M. Wagih, N. Hillier, S. Yong, A. S. Weddell and S. Beeby, "RF-powered wearable energy harvesting and storage module based on e-textile coplanar waveguide rectenna and supercapacitor," *IEEE Open J. Antennas Propag.,* vol. 2, pp. 302–314, 2021.

[51] Wires.co.uk, Litz wire, reference number: LZ00400036-500. (Feb. 14, 2023) [Online]. Available: https://www.wires.co.uk/acatalog/litzwire.html

[52] Boots, Boots cotton crepe bandage BP (10 cm x 4.5 m). (Feb. 14, 2023) [Online]. Available: https://www.boots.com/boots-cotton-crepe-bandage-bp-10cm-x-4-5m-10112503

[53] Autodesk, Eagle. [Online]. Available: https://www.autodesk.com/.

[54] Barnyarns, Vlieseline - firm fusible interlining - variable widths (SKU: VIL-2VS520-M). [Online]. Available: https://www.barnyarns.co.uk/vlieseline-grey-firm-soft-iron-on-interlining-30cm-per-metre.htmlproduct-details-tab-description.

[55] ALFA-G, Prym spray adhesive for temporary gluing of fabric and paper (Ref. Prym 968060). [Online]. Available: https://alfag.co.uk/product/prym-spray-adhesive-for-temporary-gluing-of-fabric-and-paper/.

[56] PFAFF, Creative 3.0 sewing and embroidery machine. [Online]. Available: https://shop.pfaff.com/en-us/machines/creative-30-sewing-and-embroidery-machine

[57] GeneSiC semiconductor, energy efficiency through innovation. [Online]. Available: https://www.genesicsemi.com/.

[58] M. Wagih, A. Komolafe, A. S. Weddell and S. Beeby (2022), "A wearable all-printed textile-based 6.78 MHz 15 W-output wireless power transfer system and its screen-printed joule heater application," TechRxiv. Preprint. https://doi.org/10.36227/techrxiv.21402000.v1

[59] Texas Instruments. (May 10, 2022). LM2704: micropower step-up dc/dc converter with 550 mA peak current limit. [Online]. Available: https://www.ti.com/product/LM2704.

[60] Microchip. (May 10, 2022). ATtiny85. [Online]. Available: https://www.microchip.com/en-us/product/ATtiny85.

[61] Microchip. (May 10, 2022). MCP1801. [Online]. Available: https://www.microchip.com/en-us/product/MCP1801.

[62] Vishay. (May 10, 2022). VLMU35CL2.-275-120. [Online]. Available: https://www.vishay.com/leds/list/product-80254/.

[63] Adafruit. (May 10, 2022). WS2811 NeoPixel LED driver chip. [Online]. Available: https://www.adafruit.com/product/1378.

[64] A. Komolafe, et al., "Integrating flexible filament circuits for e-textile applications," *Adv. Mater. Technol.*, vol. 4, no. 7, p. 1900176, 2019.

[65] A. Valavan, A. Komolafe, N. Harris and S. Beeby, "Encapsulation process and materials evaluation for e-textile gas sensor," *Proceedings*, vol. 32, no. 1, 2019.

[66] M. Wagih, Y. Wei, A. Komolafe, R. Torah and S. Beeby, "Reliable UHF long-range textile-integrated RFID tag based on a compact flexible antenna filament," *Sensors*, vol. 20, p. 3435, 2020.

[67] Covestro solution center, Platilon®TPU films: versatility few limitations. (Aug. 14, 2022) [Online]. Available: https://solutions.covestro.com/en/brands/platilon.

[68] Y. Zhang, Z. Zhao and K. Chen, "Frequency-splitting analysis of four-coil resonant wireless power transfer," *IEEE Trans. Ind. Appl.*, vol. 50, no. 4, pp. 2436–2445, July-Aug. 2014.

[69] D. Vital, P. Gaire, S. Bhardwaj and J. L. Volakis, "An ergonomic wireless charging system for integration with daily life activities," *IEEE Trans Microw. Theory Tech.,* vol. 69, no. 1, pp. 947–954, Jan. 2021.

[70] A. Hajiaghajani et al., "Textile-integrated metamaterials for near-field multibody area networks," *Nat. Electron.,* vol. 4, pp. 808–817, 2021.

[71] V. Mishra and A. Kiourti, "Wearable planar magnetoinductive waveguide: a low-loss approach to WBANs," IEEE Trans. Antennas Propag., vol. 69, no. 11, pp. 7278–7289, Nov. 2021.

[72] ITIS foundation, Tissue properties. (Aug. 14, 2022) [Online]. Available: https://itis.swiss/virtual-population/tissue-properties/database/.

[73] Comsol multiphysics. (Aug. 14, 2022) [Online]. Available: https://www.comsol.com/.

[74] GaN systems, evaluation board: GSWP050W-EVBPA. [Online]. Available: https://gansystems.com/evaluation-boards/gswp050w-evbpa/.

[75] B. R. Das, "UV radiation protective clothing," *The open textile journal*, vol. 3, pp. 14–21, 2010.

[76] Vishay, UVC emitting diode in SMD Package, VLMU35CL2.-275-120 datasheet, 10 Sep. 2020 [Revised 01 Jan. 2022].

[77] P. Li et al., "Mitigation of airborne PRRSV transmission with UV light treatment: proof-of-concept," *Agriculture,* vol. 11, no. 3, pp. 259, 2021.

[78] C. Holmström and S. Kjelleberg, "Marine Pseudoalteromonas species are associated with higher organisms and produce biologically active extracellular agents," *FEMS Microbiol. Ecol.*, vol. 30, pp. 285–293, 1999.

[79] Centers for disease control and prevention. (Sept. 27, 2022). Gram negative bacteria infections in healthcare settings. [Online]. Available: https://www.cdc.gov/hai/organisms/gram-negative bacteria.html.

[80] G. L. Klein, E. Soum-Soutéra, Z. Guede, A. Bazire, C. Compère and A. Dufour, "The anti-biofilm activity secreted by a marine Pseudoalteromonas strain," *Biofouling*, vol. 27, no. 8, pp. 931–940, 2011.

[81] C. M. Pradier, C. Rubio, C. Poleunis, P. Bertrand, P. Marcus and C. Compere, "Surface characterization of three marine bacterial strains by fourier transform IR, X-ray photoelectron spectroscopy, and time-of-flight secondary-ion mass spectrometry, correlation with adhesion on stainless steel surfaces," *J. Phys. Chem. B*, vol. 109, no. 19, pp. 9540–9549, 19 May 2005.

[82] C. Leroy, C. Delbarre-Ladrat, F. Ghillebaert, C. Compere and D. Combes, "Effects of commercial enzymes on the adhesion of a marine biofilm-forming bacterium," *Biofouling*, vol. 24, no. 1, pp. 11–22, 2008.

[83] C. Leroy, C. Delbarre-Ladrat, F. Ghillebaert, C. Compere and D. Combes, "Influence of subtilisin on the adhesion of a marine bacterium which produces mainly proteins as extracellular polymers," *J. Appl. Microbiol.*, vol. 105, no. 3, pp. 791–799, 2008.

[84] E. Heo, K-Y. Choi, J. Kim, J-H. Park, H. Lee, "A wearable textile antenna for wireless power transfer by magnetic resonance," *Tex. Res. J.*, vol. 88, no. 8, pp. 913–921, 2018.

[85] Y. Li, N. Grabham, R. Torah, J. Tudor, S. Beeby, "Textile-based flexible coils for wireless inductive power transmission," *Appl. Sci.*, vol. 8, no. 6, pp. 912, 2018.

[86] S. Jeong et al., "Smartwatch strap wireless power transfer system with flexible PCB coil and shielding material," *IEEE Trans. on Ind. Electron.*, vol. 66, no. 5, pp. 4054–4064, May 2019.

[87] G. Xu et al., "Battery-free and Wireless Smart wound dressing for wound infection monitoring and controlled on-demand drug delivery," *Adv. Funct. Mater.*, vol. 21, no. 26, p. 2100852, 2021.

[88] T. Ning et al., "Highly efficient self-healing multifunctional dressing with antibacterial activity for sutureless wound closure and infected wound monitoring," *Adv. Mater.*, vol. 34, no. 3, p. 2106842, 2021.

[89] P. Mostafalu et al., "Smart bandage for monitoring and treatment of chronic wounds," *Small*, vol.14, no. 33, p. 1703509, 2018.

[90] Q. Pang, L. Dong, L. Shijian, W. Guangming, Q. Bianbian, D. Shurong, M. Lie, G. Changyou and W. Zhaohui, "Smart flexible electronics-integrated wound dressing for real-time monitoring and on-demand treatment of infected wounds," *Adv. Sci.*, vol. 7, no. 6, pp. 1902673, 2020.

[91] Y. Cai et al., "Multifunctional zwitterionic microneedle dressings for accelerated healing of chronic infected wound in diabetic," *Biomater. Sci.*, 2023.

[92] C. Leroy et al., "A marine bacterial adhesion microplate test using the DAPI fluorescent dye: a new method to screen antifouling agents," *Appl. Microbiol.*, vol. 44, no. 4, pp. 372–378, Feb. 2007.

Irfan Ullah is a Research Fellow in the Smart Electronics and Material Group, School of Electronics and Computer Science at the University of Southampton, UK. He obtained his B.Eng. degree in Electronic and Communications Engineering in 2016 and PhD degree in Electronic Engineering in 2020 from the University of Kent, UK. His current research interests include passive UHF RFID tags, small antennas, wireless power transfer and smart bandages for healthcare applications.

Mahmoud Wagih (GS'18, M'21) received his B.Eng. (Hons.) in September 2018, and his Ph.D. on rectenna design in April 2021, both in Electrical and Electronic Engineering from the University of Southampton.

He is currently a UK IC Research Fellow and Proleptic Lecturer (Assistant Professor) at the University of Glasgow. His interests broadly RF and antenna-enabled sustainable electronics including energy harvesting, sensing, and wearable applications.

Dr. Wagih was the recipient of 15+ awards including the "EurAAP" Per-Simon Kildal Award for the Best PhD in Antennas and Propagation and the Best in Engineering and Physical Sciences Doctoral Research Award at the University of Southampton. He received the Best Student Paper Award at the IEEE Wireless Power Transfer Conference, 2019, the Best Oral Presentation at PowerMEMS, 2019, the Best Paper Award at PowerMEMS, 2021, the IEEE MTT-S Best 3MT Presentation Prize (second place) at the IEEE Microwave Week, 2020, was a U.K. TechWorks Young Engineer of the Year finalist, in 2021, and an International Union of Radio Science (URSI) Young Scientist Award, in 2022. He is a Senior Member of URSI, an affiliate member of the IEEE Microwave Theory & Technologies (MTT) Technical Committees TC-25, on Wireless Power, and a member of MTT TC-26, on RFID, Wireless Sensor, and IoT.

Yixuan Sun received the B.Eng (First Class Hons.) degree in electrical and electronic engineering from the University of Southampton, Southampton, U.K., in 2019. She is currently a PhD student in Electronics and Computer Science at the University of Southampton.

Her research interests include magnetic resonant power transfer, wireless power transfer, flexible coils, and flexible circuits for wearable applications.

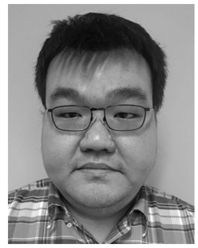

Yi Li is a Senior Research Fellow in the Smart Electronics and Material Group, School of Electronics and Computer Science at the University of Southampton, UK. He obtained his B.Eng. degree in Electronic Engineering in 2008 from the University of Warwick, his M.Sc. degree in Micro-System Technology (MST) in 2009 and his PhD degree in printed electronic components for e-textile applications in 2013 from the University of Southampton, UK.

His current research mainly focuses on functional material formulation investigation, at the same time, developing e-textile applications in printed e-textiles, for example, solar cells, light-emitting devices, and smart bandages.

Kata Hajdu is an environmental researcher specialised in water and soil purification and waste management with a PhD in biophysics. She has been involved in various multidisciplinary research projects in the environmental and medical sector for the past fourteen years. She is the author and co-author of twenty international scientific papers and eight book chapters. She has a strong and diversified background in optical biosensors, microbiology and chemical analytical technologies. After a one-year long project in Greece on the removal of organochlorinated compounds from soil, she received a three-year grant from the Hungarian Academy of Science. She was responsible for the scientific, administrative and financial areas of her project on light-harvesting biocomposites with the use of photosynthetic bacteria. In the last couple of years, she worked on the implementation of two projects on micro- and nanofluidic biosensors at LAAS, CRNS, France. She joined IFREMER in 2022 in the framework of the INTERREG project SmartT.

Rémi Courson received his M.S. degree in physical chemistry in 2007 (University of Paris 7 Denis Diderot, France) and his PhD in materials science in 2011 (University of Montpellier 2, France). From 2007 to 2012, he worked at L2C in Montpellier, France, on the synthesis of hybrid materials (sol-gel process) for microelectronics, ophthalmic optics and building insulation. In 2012, he joined LAAS-CNRS laboratory in Toulouse, France, to work on the development of photoresists compatible with standard microelectronic equipment and lamination technologies for microfluidics applications. From 2015 to 2017, he was hired by Kloé company to develop processes on a new high-resolution stereolithography (SLA) equipment. Then between 2017 and 2020, he went back to LAAS-CNRS to work in an additive manufacturing platform. He was in charge of five 3D printers and develop many processes with different materials for several research areas such as microfluidic, photonics, model for biologist (cellular microenvironment), functionalization equipment. Since November 2020, he has a research engineer position at Ifremer in the Department of Technological Research within the laboratory Detection, Sensors and Measures (DSN). He is involved in all microfluidic and/or microfabrication development led in the DSN laboratory.

Catherine Dreanno is a marine biologist with research interests in the control of marine biofouling, in chemical ecology, in reproduction and development of marine organisms and in molecular ecology. In 2008, she has joined IFREMER and focuses her research activities to biofilm formation and genomics and to the ecology of microalgae with a special emphasis on the development of new tools and sensors for molecular identification of plankton and microorganisms.

Enora Prado is an associate researcher in vibrational spectroscopies and analytical chemistry. She received a PhD degree from the University of Bordeaux, France, in 2011, for the development of quantitative RNA measurement by SERS. From 2012 to 2017, she has been involved in various multidisciplinary research projects in the medical and environmental sectors. She worked at the University of Grenoble on a screening of G-quartet DNA targets by SPR for one years before joining Prof. Nardin team at the University of Geneva for two years on amyloid fibers analysis. Then, she continued to work on biomimetic self-assembly at the University of Rennes, France, before developing a prediction model of fatty acids composition in the rainbow trout Oncorhynchus mykiss by using Raman micro-spectroscopy. Since 2019, she is an associate researcher at IFREMER (National Institute for Ocean Science, France). Her current research mainly focuses on optical (bio)-sensors development (surface chemistry, development and validation of analytical protocols) and micro-plastics identification by raman imaging.

Abiodun Komolafe received the B.Sc. degree (Hons.) in physics from the University of Ibadan, Nigeria, in 2007, and the M.Sc. degree in microelectromechanical systems and the Ph.D. degree in printed circuits on fabrics from the University of Southampton, in 2011 and 2016, respectively. He is currently working as a Research Fellow with the University of Southampton, in investigating novel manufacturing methods for making functional electronics on textiles using flexible electronic circuits and screen printed electronics for medical applications. He is experienced in the design and fabrication of e-textiles using screen printing and thin film technologies

Nick R. Harris is currently a Professor with the Electronics and Computer Science Department, University of Southampton, Southampton, U.K., where he is involved in novel sensors and sensor systems, wireless sensor networks, microfluidic systems, ultrasonic particle manipulation, sonoporation and electroporation of cells, and energy harvesting, with funding from the EU, EPSRC, BBSRC, and industry. He is also a Chartered Engineer and a Co-Founder of Perpetuum Ltd., Romsey, U.K. He has authored or coauthored over 200 publications and patents in these fields. His current research interests include sensors for rehabilitation systems, distributed sensors for agriculture and environmental monitoring, machine-learning approaches for distributed sensor systems, self-powered health and usage monitors, embedded condition-monitoring microsystems, ion-selective electrochemical sensors, and novel environmental energy harvesters.

Prof. Harris is a member of the Institution of Engineering and Technology.

Neil M. White (M'01, SM'02) received a PhD degree from the University of Southampton, Southampton, UK, in 1988, for a thesis describing the piezoresistive effect in thick-film resistors. He was appointed as a lecturer within the School of Electronics and Computer Science in 1990 and promoted to senior lecturer in 1999 and reader in 2000, and he was awarded a Personal Chair in 2002. Professor White was Head of the School of Electronics and Computer Science from 2011 to 2015. He lectures on electronic circuits, micro-electro-mechanical systems, and advanced instrumentation and sensors. He has co-authored several textbooks and has published more than 250 peer-reviewed scientific papers in the area of sensors and energy harvesting systems. He is a former director and co-founder of the university spin-out company Perpetuum Ltd., which specializes in vibration energy harvesting. He was the recipient of the 2009 Calendar Silver Medal, awarded by the Institute of Measurement and Control for his outstanding contribution to the art of instruments and measurement

Steve Beeby (Fellow, IEEE) received the B.Eng. (Hons.) degree in mechanical engineering from the University of Portsmouth, Portsmouth, U.K., in 1992, and the Ph.D. degree in MEMS resonant sensors from the University of Southampton, Southampton, U.K., in 1998. He is currently the Director of the Centre for Flexible Electronics and E-Textiles and leads the U.K.'s E-Textiles Network. He is currently leading three U.K. funded research projects and has received over 20 million research funding. He is a co-founder of Perpetuum Ltd., a University spin-out based upon vibration energy harvesting formed in 2004, Smart Fabric Inks Ltd., and D4 Technology Ltd. He has coauthored/edited four books including Energy Harvesting for Autonomous Systems (Artech House, 2010). He has given over 30 plenary/keynote/invited talks and has over 350 publications and an H-Index of 56. His current research interests focus on energy harvesting, e-textiles and the use of energy harvesting in wearable applications. Prof. Beeby was the recipient of two prestigious EPSRC Research Fellowships to investigate the combination of screen-printed active materials with micromachined structures and textiles for energy harvesting and was also awarded a Personal Chair in 2011. He has most recently been awarded a prestigious RAEng Chair in Emerging Technologies in E-textile Engineering.